

Coexistence of Weyl semimetal and Weyl nodal loop semimetal phases in a collinear antiferromagnet

Jie Zhan,^{1,2} Jiangxu Li,² Wujun Shi,^{3,4} Xing-Qiu Chen,^{1,2,*} and Yan Sun^{1,2,†}

¹*School of Materials Science and Engineering, University of Science and Technology of China, Shenyang, China.*

²*Shenyang National Laboratory for Materials Science,*

Institute of Metal Research, Chinese Academy of Sciences, Shenyang, China.

³*Center for Transformative Science, ShanghaiTech University, Shanghai 201210, China*

⁴*Shanghai High Repetition Rate XFEL and Extreme Light Facility (SHINE), ShanghaiTech University, Shanghai 201210, China*

Antiferromagnets (AFMs) with anomalous quantum responses have lead to new progress for the understanding of their magnetic and electronic structures from symmetry and topology points of view. Two typical topological states are the collinear antiferromagnetic Weyl semimetal (WSM) and Weyl nodal loop semimetal (WNLSM). In comparison with the counterparts in ferromagnets and non-collinear AFMs, the WSMs and WNLSMs in collinear AFMs are still waiting for experimental verification. In this work, we theoretically predicted the coexistence of Weyl points (WPs) and Weyl nodal loops (WNLs) in transition metal oxide RuO₂. Owing to the small magnetocrystalline anisotropy energy, the WPs and WNLs can transform to each other via tuning the Néel vector. Moreover, since the WPs are very close to Fermi level and the WNLs are even crossing Fermi level, the topological states in RuO₂ can be easily probed by photoemission and STM methods. Our result provides a promising material platform for the study of WSM and WNLSM states in collinear AFMs.

I. BACKGROUND AND INTRODUCTION

Recently, the understanding of magnetic structures in antiferromagnets (AFMs) was refreshed according to the symmetry constraint quantum transport properties and topological band structures [1–18]. Generally, a material with magnetic order and zero net magnetic moment is considered as an AFM, in which the zero net moment makes it not sensitive to external magnetic field. With the progress of understanding in quantum responses (such as anomalous Hall effect (AHE) and spin-orbital torque (SOT), et al.), some antiferromagnetic structures get intensive interest since they can host some quantum responses that were believed to only exist in ferromagnetic and ferrimagnetic counterparts with non-zero net magnetizations [1–4].

A typical example is the non-collinear AFM. Though the theoretical prediction of AHE was as early as 2001 [1], its experimental realization was only achieved after around 15 years later [6]. After that, the non-collinear AFM gets extensive attention due to their exotic transport properties and topological band structures. The observation of AHE [6, 7], anomalous Nernst effect (ANE) [19, 20] and magneto-optical responses [21, 22] inspired the further understanding of collinear AFM. Accordingly, the collinear AFM can be further classified into two groups that with and without AHE [16].

Though the existence of intrinsic AHE needs to break time-reversal symmetry, most collinear AFMs can be viewed as two sublattices that are connected by the joint

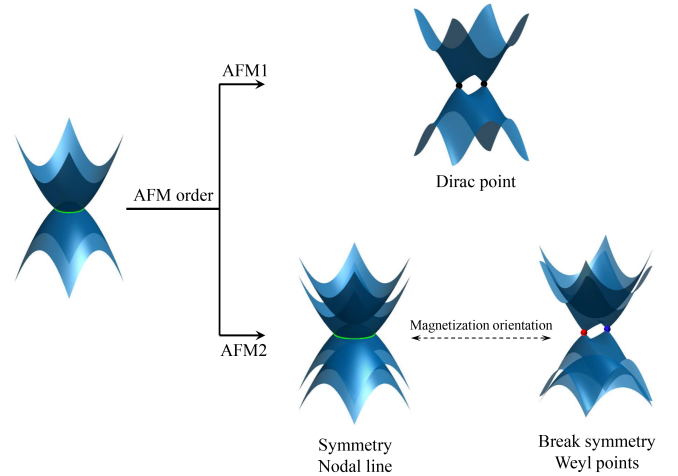


FIG. 1. Schematic of possible topological band structures in collinear antiferromagnets (AFMs). In the case of AFM1 with either PT or $\{T|\tau\}$ symmetry, the linear touching points of electronic band structure are at least four-fold degenerate in the form of Dirac points. In the cases of AFM2 in the absence of PT or $\{T|\tau\}$ symmetries, both doubly degenerate Weyl points (WPs) and Weyl nodal loops (WNLs) are allowed. Their existence can be controlled via the magnetization orientation.

space group and time-reversal operations. Such symmetries can lead to the cancellation of Berry curvature in the whole Brillouin zone (BZ) and therefore the AHE is forbidden. Another consequence of the joint symmetry is the spin degeneracy in band structures, with which the four-fold Dirac points are allowed [23, 24] but that with lower-fold-degeneracy are forbidden by symmetry, see the up panel of Fig. 1

* xingqiu.chen@imr.ac.cn

† sunyan@imr.ac.cn

On the other hand, a finite non-zero anomalous Hall conductivity (AHC) is symmetrically allowed if such kind of joint symmetry is absent and it is usually along with band spin split. It allows topological band structures with odd-number-fold degeneracy in collinear AFMs, where two typical doubly degenerate linear crossing states are Weyl point (WP) and Weyl nodal loop (WNL) with non-zero Chern numbers [25–30]. Together with spin-orbital coupling (SOC) and specific magnetization orientation, the topological states can be transferred between WPs and WNLs, see the bottom panel in Fig. 1.

With the development of magnetic topological materials, magnetic WSMs were experimentally verified in ferromagnet $\text{Co}_3\text{Sn}_2\text{S}_2$ [31–35], non-collinear AFM $\text{Mn}_3\text{Sn}/\text{Ge}$ [9, 36], as well as canted AFM YbMnBi_2 [37]. Besides, magnetic WNLs were also directly observed in ferromagnet Co_2MnGa [38] by ARPES measurements.

In comparison, despite both WPs and WNLs are allowed in collinear AFMs, none of them were experimentally observed, so far. The main reason maybe due to the complicated metallic electronic structure with several bands crossing Fermi level and WPs/WNLs far away from Fermi level, making them hard to detect in experimental measurements [12]. In this work, we find the co-existence of WPs and mirror symmetry protected WNLs in transition metal oxide RuO_2 . With WNLs crossing Fermi level and WPs only around 0.03 eV below Fermi level, it provides a model material platform for the direct photoemission and STM measurements.

II. METHOD

To analyze the topological properties, we calculated the electronic band structure of RuO_2 based on density functional theory by full-potential local-orbital code (FPLO) with local basis [39]. Similar to previous calculations, the correlation effect of Ru-4d orbitals are considered by the effective on-site Hubbard U , with $U=2$ eV [16, 18, 40]. To calculate the Berry curvature related topological invariants and surface states, we mapped the Bloch wavefunctions into symmetry conserving maximally projected Wannier functions [41] and constructed effective tight-binding model Hamiltonians by the Wannier functions overlap.

III. RESULTS AND DISCUSSION

RuO_2 is one of the most promising AFM AHE materials [16, 42], in which the magneto-optical response can be also manipulated by the orientation of magnetization and crystal chirality [18]. It is also the main motivation for us to choose RuO_2 as a typical example to study the WSM and WNL phases in collinear AFMs. RuO_2 has a rutile-type lattice structure belonging to space group $P4_2/mnm$ (No.136), see Fig. 2(a). The symmetry is reduced by the magnetic order, depending on the specific

spin orientation.

The magnetization is originated from the 4d orbitals on Ru sites, with easy axis along the [001] direction [43, 44]. Fig. 2(c-d) shows the energy dispersion of RuO_2 without and with the consideration of SOC. In the absence of joint PT symmetry and $\{T|\tau\}$ symmetry (with inversion operation P , time-reversal operation T , and fractional translation operation τ) that connect two magnetic sublattices, spin-up and spin-down channels are not degenerate in the band structure, consistent with previously reports [16, 18]. Since the two Ru sites are connected by a screw rotation operation $S_{4z} = \{C_{4z}|(1/2, 1/2, 1/2)\}$, the bands from two spin channels are connected by a S_{4z} operation.

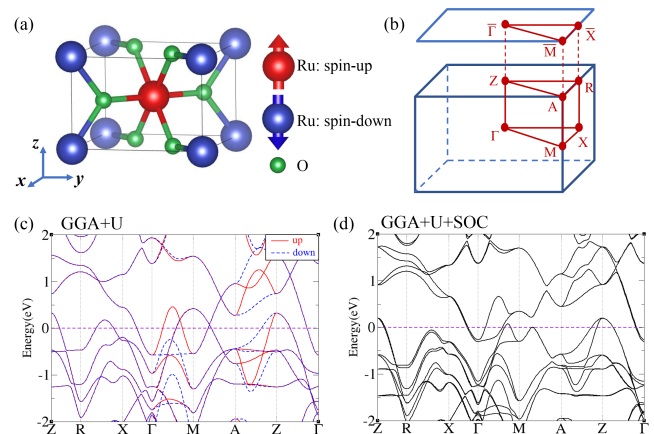


FIG. 2. Crystal and electronic structure of RuO_2 . (a) Magnetic structure of RuO_2 . (b) Three-dimensional Brillouin zone (BZ) for the tetragonal crystal lattice and its two-dimensional projection in (001) surface. (c,d) Energy dispersion of RuO_2 without and with the consideration of spin-orbital coupling (SOC).

In the case without considering SOC, the system follows the spin rotation symmetry, and all the mirror symmetries and glide mirror symmetries are preserved. With the protection of mirror plane m_{001} , the band inversion in both spin-up and spin-down channels can form doubly degenerate nodal loops in the mirror invariant plane, $k_z = 0$. As presented in Fig. 3(a), the nodal rings in $k_z = 0$ plane can extend around half of the BZ in the k space. Moreover, the nodal loops cut Fermi level with strong dispersions, where the energy windows are in the range of ~ -0.3 eV to ~ 0.2 eV, see the color bar labeled nodal loops in Fig. 3(a) and three dimensional energy dispersions in Fig. 3(b).

In addition, the other mirror symmetries of m_{110} and m_{1-10} also lead to nodal loops in $k_x - k_y = 0$ and $k_x + k_y = 0$ planes, respectively, and they touch the nodal loops in $k_z = 0$ plane on the Γ -M line. But the nodal loops in $k_x \pm k_y = 0$ are around 0.15 eV above Fermi level and not easy to detect in experiments. Owing to the screw rotation operation that connects two Ru-sites, the nodal loops

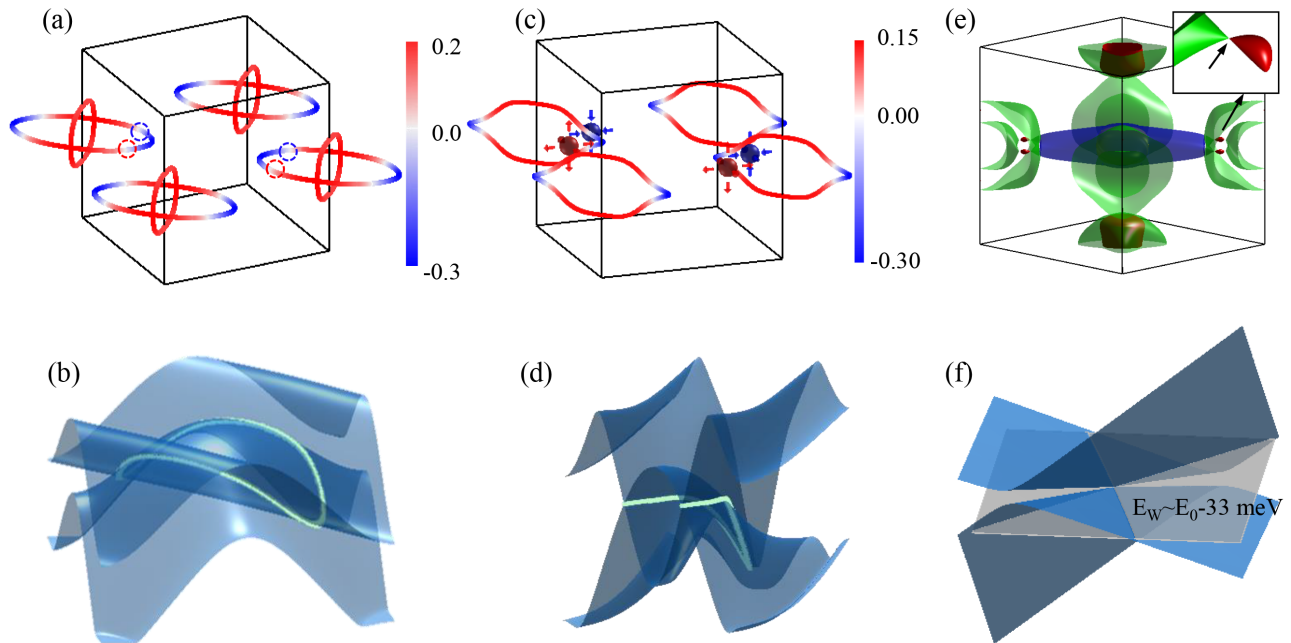


FIG. 3. WPs and nodal loops in RuO_2 . (a) Location of nodal loops from spin-up channel in the case without considering SOC. The dashed circles represent the location of WPs after consideration of SOC. The red and blue colors for the dashed circles indicates the chirality of WPs. (b) Corresponding three dimensional energy dispersion of the nodal loop in $k_z=0$ plane. (c) Location of WPs and WNLs in the case of including SOC, with magnetization orientation along $[110]$. (d) Energy dispersion of the WNL (e) Fermi surface of RuO_2 with energy lying at E_W . (f) Energy dispersion around WP. The color bar is in the unit of eV, 0 eV is the Fermi level.

from spin-up channel around the $(-\pi, \pi, 0)$ corner and that from spin-down channel around the $(\pi, \pi, 0)$ corner are linked by a C_{4z} rotation operation.

With the inclusion of SOC, the existence and behavior of the original nodal rings depend on the specific magnetization orientations, see the sketch in Fig. 1. When the Néel vector is perpendicular to the plane, the original nodal loops can be preserved if the wavefunctions of the two bands have opposite mirror eigenvalues. Otherwise, the gapless linear crossing will be broken with opening band gaps, and WPs are allowed nearby. Meanwhile, when SOC is taken into consideration, the hybridization of two spin channels can generate additional WNLs and WPs.

We noted that previous *ab-initio* calculations found the magnetocrystalline anisotropy energy is only around 2.76 meV/Ru [18]. Such small energy difference illustrates the easy tunability of the Néel vector. Weak doping in the form of $\text{Ru}_{1+x}\text{O}_{2-x}$ and $\text{Ru}_{1-x}\text{Ir}_x\text{O}_2$ can change the Néel vector to lying within (001) plane [16]. Recently experimentally grown $[001]$ oriented RuO_2 thin films have the in-plane magnetization [42]. Therefore, most studies about the electrical and optical responses focused on the cases with in-plane Néel vector. With tiny hole-doping, the AHC can reach up to ~ 300 S/cm [16], a big value in all AMFs. In linear magneto-optical response, both Kerr rotation angle and Faraday rotation

angle increase along with rotating Néel vector away from $[001]$ axis to (001) plane, and the peak value can reach up to ~ 0.6 and ~ 2.0 degree, respectively [18].

Considering the strong non-trivial quantum responses of RuO_2 mainly happen in the cases with magnetization in (001) plane [16, 18], we will also focus on the same situations. Taking magnetization along $[110]$ as an example, the magnetic structure breaks most of the mirror symmetries, and only m_{110} is left. Therefore the WNLs are only allowed in the (110) plane, namely, in the planes satisfying $k_x + k_y = 0$ or $k_x + k_y = \pi$.

As presented in Fig. 3(c), one independent WNL exists in the $k_x + k_y = 0$ plane, which can extend around half of the BZ. With doubly degenerate linear crossing, the WNL hosts a π Berry phase for the Wilson loop around it. Nearby the hinge of BZ with $k_x = k_y = \pi$, the WNL is almost flat with very weak dispersion. A sharp dispersion appears away from the hinge, with energy window in the range of -0.3 eV to 0.15 eV, crossing the Fermi level. This WNL is constructed by the bands with opposite spin orientations and does not exist in the situation without considering SOC.

In addition to the WNLs, we also find one pair of independent WPs with opposite chiralities in $k_z = 0$ plane. The WPs are originated from the nodal rings in Fig. 3(a) in the case without including SOC, see the red and blue dashed circles. The $[110]$ oriented magnetiza-

tion together with SOC break the original mirror symmetry m_z . Hence, the gapless nodal loops were broken with opening band gaps. Meanwhile, the WPs are formed on the the original nodal loops, similar to the situation in $\text{Co}_3\text{Sn}_2\text{S}_2$ [31–33]. Considering the inversion symmetry, there are four WPs near Fermi level in the 1st BZ in total, see Fig. 3(a). Since the location of WP is close to the Fermi cutting between the original nodal rings and Fermi energy, this pair of WPs are very close to Fermi level, with an energy of $E \sim E_0 - 0.03$ eV, making them very easy to detect by the surface measuring techniques, such as ARPES and STM. We further checked the Fermi surface by fixing the energy at WP and found that it also presents as a linear touching of the Fermi surfaces. As shown in Fig. 3(e), there are four Fermi surfaces at $E = E_W$, consistent with the energy dispersion plotted in Fig. 2(d). Owing to the PT and $\{T|\tau\}$ symmetry breaking and strong local magnetization on Ru sites, all the Fermi surfaces are with large spin split, except for some high symmetry points and the special doubly degenerated WPs. As presented in the upper-right corner of Fig. 3(e), the WP presents as a linear touching of one small red bubble and one large green bubble from original spin-up channel.

Correspondingly, the energy dispersion is strongly tilted near the WPs. The constant energy plane at E_W cuts both electron and hole bands through the linear crossing point, see Fig. 3(f). Therefore, it is a typical type-II WP [45, 46]. Rotating the Néel vector from [110] to [100] in (001) plane or from [110] to [001] in (1-10) plane, the positions of WPs are also shifting in both energy and k spaces. In some specific angles, they are canceled out in the situation of meeting the other WP with opposite chirality.

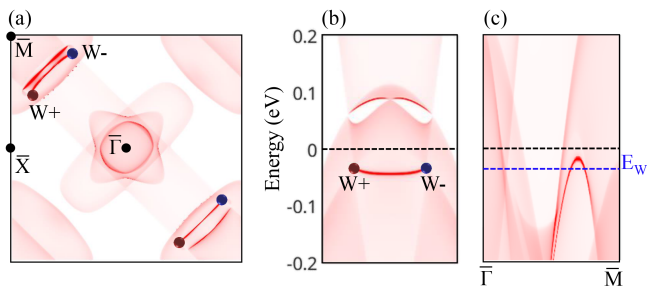


FIG. 4. Surface states of RuO_2 . (a) Fermi surface with energy lying at WP. (b) Energy dispersion crossing one pair of WPs with opposite chirality. (c) Energy dispersion along $\bar{\Gamma} - \bar{M}$. Red and white color demonstrate the occupied and unoccupied states, respectively.

A typical feature of the WSM is the existence of non-closed topological surface Fermi arc [25]. To calculate the

surface state, we considered a half-infinite open boundary condition along [001] direction by the Green’s function method [47, 48]. Putting the energy at the E_W , one can easily see a Fermi arc surface state connecting two WPs with opposite chiralities, see Fig. 4(a). Though the bulk magnetic structure of RuO_2 has inversion symmetry, the top or bottom surfaces does not follow it after cutting bulk chemical bonding. Hence, these two Fermi arcs near $(-\pi/a, \pi/a)$ and $(\pi/a, -\pi/a)$ are not connected by any symmetries and their detailed shapes are different. The Fermi arc states are further confirmed by the energy dispersion along the line crossing one pair of WPs. The surface band starts from the bulk linear crossing point ($W+$) and ends at the other one ($W-$), see Fig. 4(b).

In addition to the above Fermi arc, one can see the other surface state almost parallel to the Fermi arc, which merges into bulk states at the ends. At first glance, it also shows a Fermi arc feature. To see the physical origin of this surface state, we plot the surface energy dispersion along $\bar{\Gamma} - \bar{M}$, by crossing the connection of two WPs. As presented in Fig. 4(c), both of them indeed belong to the same surface band and the constant energy E_W cuts this band twice. Therefore, both of them are parts of the Fermi arcs. In principle, there should be an odd number of Fermi crossings with only one pair of WPs. But because of the complicated bulk band overlap, there is not an indirect band gap between $\bar{\Gamma} - \bar{M}$ and some surface states are merged into bulk, making the other Fermi crossings not visible.

IV. SUMMARY

In summary, we systematically understand the topological band structure in collinear AFM RuO_2 from first-principle calculations and symmetry analysis. In absent of joint PT and $\{T|\tau\}$ symmetries, WPs and WNLs can coexist in RuO_2 and they can transform to each other via magnetization orientation. Furthermore, the WPs are only around 30 meV below Fermi level and the WNLs cut Fermi level. After the discovery of WSMs and WNLs in ferromagnets and non-collinear AFMs, RuO_2 provides a promising material platform for direct observation of WPs and WNLs in collinear AFMs.

ACKNOWLEDGMENTS

This work was supported by the National Science Fund (Grant No. 51725103, 52188101) and Jiangxu Li acknowledges the support from the fellowship of China Postdoctoral Science Foundation (Grant No. 2021M700152).

[1] R. Shindou and N. Nagaosa, Phys. Rev. Lett. **87**, 116801 (2001).

[2] H. Chen, Q. Niu, and A. H. MacDonald, Phys. Rev. Lett. **112**, 017205 (2014).

- [3] J. Kübler and C. Felser, *EPL (Europhysics Letters)* **108**, 67001 (2014).
- [4] J. Železný, H. Gao, K. Vybírný, J. Zemen, J. Mašek, A. Manchon, J. Wunderlich, J. Sinova, and T. Jungwirth, *Physical review letters* **113**, 157201 (2014).
- [5] W. Feng, G.-Y. Guo, J. Zhou, Y. Yao, and Q. Niu, *Physical Review B* **92**, 144426 (2015).
- [6] S. Nakatsuji, N. Kiyohara, and T. Higo, *Nature* **527**, 212 (2015).
- [7] A. K. Nayak, J. E. Fischer, Y. Sun, B. Yan, J. Karel, A. C. Komarek, C. Shekhar, N. Kumar, W. Schnelle, J. Kübler, C. Felser, and S. S. P. Parkin, *Sci. Adv.* **2**, e1501870 (2016).
- [8] P. Wadley, B. Howells, J. Zelezny, C. Andrews, V. Hills, R. P. Champion, V. Novak, K. Olejnik, F. Maccherozzi, S. S. Dhesi, S. Y. Martin, T. Wagner, J. Wunderlich, F. Freimuth, Y. Mokrousov, J. Kunes, J. S. Chauhan, M. J. Grzybowski, A. W. Rushforth, K. W. Edmonds, B. L. Gallagher, and T. Jungwirth, *Science* **351**, 587 (2016).
- [9] H. Yang, Y. Sun, Y. Zhang, W.-J. Shi, S. S. Parkin, and B. Yan, *New Journal of Physics* **19**, 015008 (2017).
- [10] J. Železný, Y. Zhang, C. Felser, and B. Yan, *Physical Review Letters* **119**, 187204 (2017).
- [11] W. Shi, L. Muechler, K. Manna, Y. Zhang, K. Koepnik, R. Car, J. Van Den Brink, C. Felser, and Y. Sun, *Physical Review B* **97**, 060406 (2018).
- [12] N. J. Ghimire, A. Botana, J. Jiang, J. Zhang, Y.-S. Chen, and J. Mitchell, *Nature Communications* **9**, 1 (2018).
- [13] J. Noky and Y. Sun, *Applied Sciences* **9**, 4832 (2019).
- [14] Y. Zhang, T. Holder, H. Ishizuka, F. de Juan, N. Nagaosa, C. Felser, and B. Yan, *NATURE COMMUNICATIONS* **10** (2019).
- [15] H. Xu, J. Wei, H. Zhou, J. Feng, T. Xu, H. Du, C. He, Y. Huang, J. Zhang, Y. Liu, *et al.*, *Advanced Materials* **32**, 2000513 (2020).
- [16] L. Šmejkal, R. González-Hernández, T. Jungwirth, and J. Sinova, *Science advances* **6**, eaaz8809 (2020).
- [17] W. Feng, J.-P. Hanke, X. Zhou, G.-Y. Guo, S. Blügel, Y. Mokrousov, and Y. Yao, *Nature communications* **11**, 1 (2020).
- [18] X. Zhou, W. Feng, X. Yang, G.-Y. Guo, and Y. Yao, *Physical Review B* **104**, 024401 (2021).
- [19] M. Ikhlas, T. Tomita, T. Koretsune, M.-T. Suzuki, D. Nishio-Hamane, R. Arita, Y. Otani, and S. Nakatsuji, *Nature Physics* **13**, 1085 (2017).
- [20] X. Li, L. Xu, L. Ding, J. Wang, M. Shen, X. Lu, Z. Zhu, and K. Behnia, *Physical Review Letters* **119**, 056601 (2017).
- [21] T. Higo, H. Man, D. B. Gopman, L. Wu, T. Koretsune, O. M. van't Erve, Y. P. Kabanov, D. Rees, Y. Li, M.-T. Suzuki, *et al.*, *Nature Photonics* **12**, 73 (2018).
- [22] Z. Liu, H. Chen, J. Wang, J. Liu, K. Wang, Z. Feng, H. Yan, X. Wang, C. Jiang, J. Coey, *et al.*, *Nature Electronics* **1**, 172 (2018).
- [23] P. Tang, Q. Zhou, G. Xu, and S.-C. Zhang, *Nature Physics* **12**, 1100 (2016).
- [24] L. Šmejkal, J. Železný, J. Sinova, and T. Jungwirth, *Physical review letters* **118**, 106402 (2017).
- [25] X. Wan, A. M. Turner, A. Vishwanath, and S. Y. Savrasov, *Physical Review B* **83**, 205101 (2011).
- [26] H. Weng, C. Fang, Z. Fang, B. A. Bernevig, and X. Dai, *Phys. Rev. X* **5**, 011029 (2015).
- [27] S.-M. Huang, S.-Y. Xu, I. Belopolski, C.-C. Lee, G. Chang, B. Wang, N. Alidoust, G. Bian, M. Neupane, C. Zhang, S. Jia, A. Bansil, H. Lin, and M. Z. Hasan, *Nature Communications* **6**, 1 (2015).
- [28] B. Q. Lv, H. M. Weng, B. B. Fu, X. P. Wang, H. Miao, J. Ma, P. Richard, X. C. Huang, L. X. Zhao, G. F. Chen, Z. Fang, X. Dai, T. Qian, and H. Ding, *Phys. Rev. X* **5**, 031013 (2015).
- [29] S.-Y. Xu, I. Belopolski, N. Alidoust, M. Neupane, G. Bian, C. Zhang, R. Sankar, G. Chang, Y. Zhujun, C.-C. Lee, H. Shin-Ming, H. Zheng, J. Ma, D. S. Sanchez, B. Wang, A. Bansil, F. Chou, P. P. Shibayev, H. Lin, S. Jia, and M. Z. Hasan, *Science* **349**, 613 (2015).
- [30] C. Fang, Y. Chen, H.-Y. Kee, and L. Fu, *Physical Review B* **92**, 081201 (2015).
- [31] E. Liu, Y. Sun, N. Kumar, L. Muechler, A. Sun, L. Jiao, S.-Y. Yang, D. Liu, A. Liang, Q. Xu, J. Kroder, V. Sus, H. Borrmann, C. Shekhar, Z. Wang, C. Xi, W. Wang, W. Schnelle, S. Wirth, Y. Chen, S. T. B. Goennenwein, and C. Felser, *Nature Physics* **14**, 1125 (2018).
- [32] Q. Wang, Y. Xu, R. Lou, Z. Liu, M. Li, Y. Huang, D. Shen, H. Weng, S. Wang, and H. Lei, *Nature communications* **9**, 1 (2018).
- [33] Q. Xu, E. Liu, W. Shi, L. Muechler, J. Gayles, C. Felser, and Y. Sun, *Physical Review B* **97**, 235416 (2018).
- [34] N. Morali, R. Batabyal, P. K. Nag, E. Liu, Q. Xu, Y. Sun, B. Yan, C. Felser, N. Avraham, and H. Beidenkopf, *Science* **365**, 1286 (2019).
- [35] D. Liu, A. Liang, E. Liu, Q. Xu, Y. Li, C. Chen, D. Pei, W. Shi, S. Mo, P. Dudin, *et al.*, *Science* **365**, 1282 (2019).
- [36] K. Kuroda, T. Tomita, M.-T. Suzuki, C. Bareille, A. Nugroho, P. Goswami, M. Ochi, M. Ikhlas, M. Nakayama, S. Akebi, *et al.*, *Nature materials* **16**, 1090 (2017).
- [37] S. Borisenko, D. Evtushinsky, Q. Gibson, A. Yaresko, K. Koepnik, T. Kim, M. Ali, J. van den Brink, M. Hoesch, A. Fedorov, *et al.*, *Nature communications* **10**, 1 (2019).
- [38] I. Belopolski, K. Manna, D. S. Sanchez, G. Chang, B. Ernst, J. Yin, S. S. Zhang, T. Cochran, N. Shumiya, H. Zheng, *et al.*, *Science* **365**, 1278 (2019).
- [39] K. Koepnik and H. Eschrig, *Phys. Rev. B* **59**, 1743 (1999).
- [40] S. L. Dudarev, G. A. Botton, S. Y. Savrasov, C. Humphreys, and A. P. Sutton, *Physical Review B* **57**, 1505 (1998).
- [41] K. Koepnik, O. Janson, Y. Sun, and J. Brink, *arXiv preprint arXiv:2111.09652* (2021).
- [42] Z. Feng, X. Zhou, L. Šmejkal, L. Wu, Z. Zhu, H. Guo, R. González-Hernández, X. Wang, H. Yan, P. Qin, *et al.*, *arXiv preprint arXiv:2002.08712* (2020).
- [43] T. Berlijn, P. C. Snijders, O. Delaire, H.-D. Zhou, T. A. Maier, H.-B. Cao, S.-X. Chi, M. Matsuda, Y. Wang, M. R. Koehler, *et al.*, *Physical review letters* **118**, 077201 (2017).
- [44] Z. Zhu, J. Stremper, R. Rao, C. Occhialini, J. Pellicciari, Y. Choi, T. Kawaguchi, H. You, J. Mitchell, Y. Shao-Horn, *et al.*, *Physical review letters* **122**, 017202 (2019).
- [45] A. A. Soluyanov, D. Gresch, Z. Wang, Q. Wu, M. Troyer, X. Dai, and B. A. Bernevig, *Nature* **527**, 495 (2015).
- [46] Y. Sun, S. C. Wu, M. N. Ali, C. Felser, and B. Yan, *Phys. Rev. B* **92**, 161107(R) (2015).
- [47] M. P. L. Sancho, J. M. L. Sancho, and J. Rubio, *Phys. F: Met. Phys* **14** (1984).

- [48] M. P. L. Sancho, J. M. L. Sancho, and J. Rubio, Phys. F: Met. Phys **15** (1985).